Quantum critical scaling at the edge of Fermi liquid stability in a cuprate superconductor

Nicholas P. Butch[1], Kui Jin[1], Kevin Kirshenbaum, Richard L. Greene[2], and Johnpierre Paglione

Center for Nanophysics and Advanced Materials and Department of Physics, University of Maryland, College Park, MD 20742

Edited by Douglas J. Scalapino, University of California, Santa Barbara, CA, and approved March 20, 2012 (received for review December 20, 2011)

In the high-temperature cuprate superconductors, the pervasiveness of anomalous electronic transport properties suggests that violation of conventional Fermi liquid behavior is closely tied to superconductivity. In other classes of unconventional superconductors, atypical transport is well correlated with proximity to a quantum critical point, but the relative importance of quantum criticality in the cuprates remains uncertain. Here, we identify quantum critical scaling in the electron-doped cuprate material $La_{2-x}Ce_xCuO_4$ with a line of quantum critical points that surrounds the superconducting phase as a function of magnetic field and charge doping. This zero-temperature phase boundary, which delineates a metallic Fermi liquid regime from an extended non-Fermi liquid ground state, closely follows the upper critical field of the overdoped superconducting phase and gives rise to an expanse of distinct non-Fermi liquid behavior at finite temperatures. Together with signatures of two distinct flavors of quantum fluctuations, these facts suggest that quantum criticality plays a significant role in shaping the anomalous properties of the cuprate phase diagram.

A longstanding issue in the quest to understand high-temperature superconductivity in the cuprates is in regard to the nature of the underlying ground state. Exotic transport properties (1, 2) are widely considered to arise due to the nontrivial consequences of quantum criticality (3–6), resulting in a strongly correlated electronic ground state that underpins the infamous phase diagram of the cuprates (7). The recent observations of quantum oscillations in underdoped $YBa_2Cu_3O_{6+x}$ (8) have provided a significant advance to our knowledge of the progression of this ground state through the cuprate phase diagram. The presence of small Fermi surface (FS) pockets distinct from the large FS structure observed in overdoped cuprates (9) requires the existence of an FS reconstruction, which logically occurs at a quantum phase transition between ground states that modify the symmetry of the Brillouin zone. With the origin of superconductivity still under hot debate, how the phase diagram is "shaped" by the evolution of these ground states remains a crucial question.

AN FS transformation has also been directly observed in the electron-doped cuprates as a function of doping, for instance as observed in $Nd_{2-x}Ce_xCuO_4$ (10, 11). This evolution is consistent with several indications of a quantum critical point associated with the suppression of antiferromagnetic order near optimal doping for superconductivity and the appearance of a Fermi liquid (FL) ground state on the overdoped side. With relatively low upper critical field values, the electron-doped cuprates allow for a unique opportunity to study the underlying ground state of the phase diagram in much detail (12). $La_{2-x}Ce_xCuO_4$ (LCCO) is particularly unique in that its superconducting (SC) "dome" is centered at relatively lower Ce concentrations (13), making it possible to study the complete suppression of superconductivity by both doping and magnetic field. One of the most extraordinary characteristics of the cuprates is the hallmark temperature-linear resistivity, which was shown in LCCO to persist over three decades in temperature and to have a strong correlation with the pairing strength itself (14). Here, we study in detail the effects of applied magnetic field on LCCO, using the selective response of spin fluctuations and superconductivity to magnetic field and charge doping to segregate a complicated mixture of behaviors into two distinct signatures of criticality.

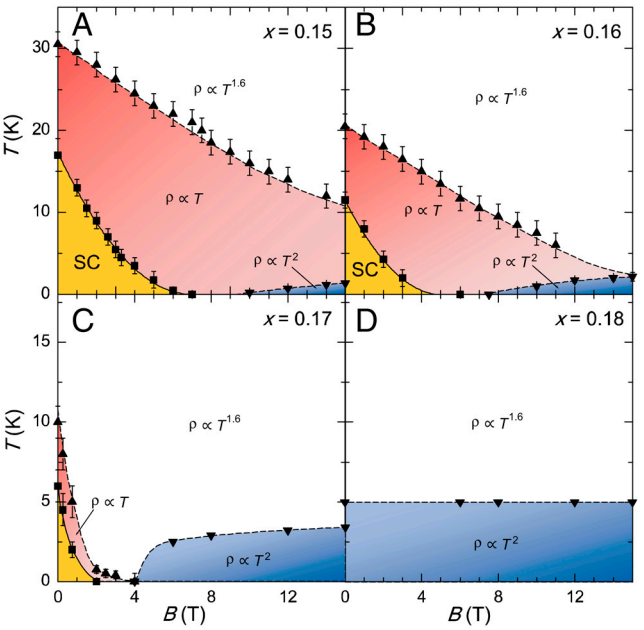

Fig. 1. Doping evolution of magnetic field-temperature phase diagrams of $La_{2-x}Ce_xCuO_4$. (*A–D*), The magnetic field dependence of the evolution of superconducting (yellow), Fermi liquid (blue), and non-Fermi liquid (red, white) ground states of the electron-doped cuprate system $La_{2-x}Ce_xCuO_4$ is shown for several electron doping levels (x). These constant-doping magnetic field (B) temperature (T) phase diagrams illustrate the interplay of two distinct transport scattering rates, represented by both $\Delta\rho \propto T$ (red regions) and $\Delta\rho \propto T^{1.6}$ (white regions) power laws, that envelope the superconducting state and characterize the non-Fermi liquid behavior emanating from the quantum critical points marking the onset of the Fermi liquid state. The crossovers between $\Delta\rho \propto T$ and $\Delta\rho \propto T^{1.6}$ scattering behavior dramatically shift with doping along with the onset field of the Fermi liquid state ($\Delta\rho \propto T^2$), indicating a strong dependence on both doping and magnetic field that persists with doping toward a dominant, field-independent state at $x = 0.18$ (*D*).

Results and Discussion

The nonsuperconducting FL ground state of overdoped LCCO can be readily accessed by either of two ways: doping in electrons beyond a critical value x_c, or increasing magnetic field above a critical value B_c that is greater than the superconducting upper

Author contributions: N.P.B., R.L.G., and J.P. designed research; N.P.B., K.J., K.K., and J.P. performed research; N.P.B., K.J., K.K., and J.P. analyzed data; and N.P.B., K.J., R.L.G., and J.P. wrote the paper.

The authors declare no conflict of interest.

This article is a PNAS Direct Submission.

[1]N.P.B. and K.J. contributed equally to this work.

[2]To whom correspondence should be addressed. E-mail: rgreene@squid.umd.edu.

This article contains supporting information online at www.pnas.org/lookup/suppl/doi:10.1073/pnas.1120273109/-/DCSupplemental.

critical field B_{c2}. Both tuning parameters suppress superconductivity and induce a FL ground state that appears to emerge continuously beyond a series of quantum critical points that evolve with both magnetic field and doping, as shown in Fig. 1. These form a continuous line along the ground state ($T = 0$) plane, constructing a dramatic landscape as a function of both doping and field, summarized in Fig. 2. A direct signature of this criticality—i.e., critical divergence as a function of an experimental tuning parameter (15)—is found as a function of magnetic field B: Upon approach to the critical field B_c from above, a divergence in the quasiparticle–quasiparticle scattering cross-section occurs as the temperature range of Fermi liquid behavior, denoted by T_{FL}, is driven to zero at B_c. At each doping the quadratic temperature coefficient A_2, determined from fits of the form $\Delta\rho = \rho - \rho_0 = A_2 T^2$ in the FL state (Fig. 3), strongly increases with decreasing field magnitude and diverges as a function of field $\Delta B = B - B_c(x)$. Furthermore, the reduced field scale $\Delta B/B_c(x)$ diverges with a universal critical exponent, $\alpha = 0.38 \pm 0.01$, that is the same for all dopings considered (Fig. 4*A*) indicating that $B_c(x)$ acts as a line of quantum critical points (*SI Text*).

Strikingly similar divergences have been identified in several different systems exhibiting magnetic field-tuned quantum criticality, including the heavy-fermion materials $CeCoIn_5$ (16), $CeAuSb_2$ (17), $YbRh_2Si_2$ (18), and $YbAlB_4$ (19), with critical exponents 1.37, 1.0, 1.0, and 0.50, respectively. In contrast to classical transitions, the sensitivity to effective dimensionality involved in a quantum phase transition can lead to nonuniversal critical exponents (15). In LCCO, the observation of a universal exponent at several doping levels is unprecedented but is limited to magnetic field tuning. When considering doping as a tuning parameter, the system can also be tuned to approach the critical field but with a distinct critical exponent. That is, A_2 also scales as a function of reduced doping $\Delta x/x_c(B)$ for different constant magnetic field values, with a critical exponent $\beta = 0.72 \pm 0.05$ (Fig. 4*B*). LCCO is a rare example of a material where both mag-

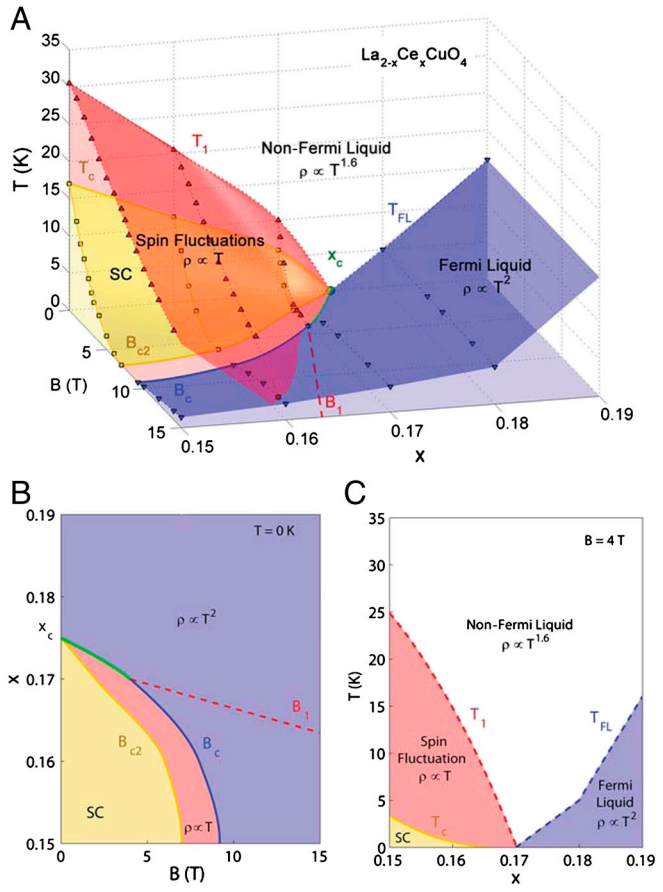

Fig. 2. Shaping of the overdoped cuprate phase diagram. (*A*) The interplay between superconducting, quantum fluctuation, and Fermi liquid phases in $La_{2-x}Ce_xCuO_4$ near the quantum critical endpoint x_c evolves as a function of electron doping (x), magnetic field (B), and temperature (T). Distinct phase boundaries between SC (yellow) and FL (blue) ground states are determined by a competition of two distinct yet related types of quantum fluctuations that give rise to separable non-Fermi liquid behavior, characterized by $\Delta\rho \propto T$ (red) and $\Delta\rho \propto T^{1.6}$ (white) resistivity temperature dependences. This behavior is found throughout the phase diagram at temperatures above the line of quantum critical points B_c (x) that extends to the zero-field critical doping x_c where the SC critical temperature T_c and cross-over temperatures T_1 and T_{FL} meet. Unconventional approximate $T^{1.6}$ scattering persists in applied magnetic fields above both the FL and SF regions, but is dominated by a linear-T scattering mechanism in the regime below T_1, where SF scattering is dominant. The origin of the SF regime is a quantum critical point at $x = 0.14$ (21). (*B*) The ground state evolution of these phases in the $T = 0$ doping-field plane exhibits a distinct separation between FL and SF ground states, with an extended non-Fermi liquid phase (red) characterized by linear-T scattering in the $T = 0$ limit. Closer to x_c, $T^{1.6}$ behavior dominates and extends to the $T = 0$ limit in a confined region (green line). Although the extrapolated limit of the SF phase B_1 (red dashed line) extends to high field, the SC upper critical field B_{c2} and the FL phase boundary B_c restrict the range of the actual SF ground state. Critical scaling behavior is associated with B_c, establishing it as a line of quantum critical points that terminates at x_c. (*C*) A constant-field cut of the phase diagram at 4 T highlights the region where the SF ground state separates the SC phase from the FL phase and $T^{1.6}$ resistivity extends to zero temperature.

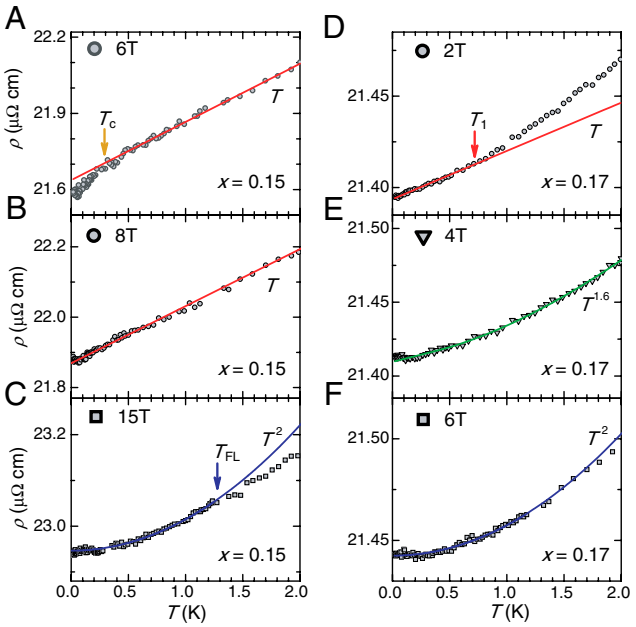

Fig. 3. Contrasting non-Fermi liquid transport behaviors. The evolution of the zero-temperature limiting behavior of electrical resistivity $\rho(T)$ for two characteristic superconducting films of $La_{2-x}Ce_xCuO_4$ with $x = 0.15$ (*A–C*) and 0.17 (*D–F*) with applied magnetic field demonstrates the isolation of two distinct non-Fermi liquid power laws. The temperature-dependent change in $\rho(T)$ is small compared to ρ_0 in all cases. (*A* and *B*) For $x = 0.15$, the suppression of the superconducting state just above 6 T reveals the extension down to the $T = 0$ limit of the ubiquitous temperature-linear resistivity associated with spin fluctuation scattering (21). (*C*) This behavior is eventually displaced by a Fermi liquid ground state with conventional approximate T^2 scattering behavior persisting up to a characteristic temperature T_{FL} (blue arrows) at higher fields. In contrast, increasing doping closer to the critical endpoint of the superconducting phase at $x_c = 0.175$ reveals a different anomalous scattering behavior. (*D*) For $x = 0.17$, the temperature-linear scattering that is present above T_c in a finite range of temperatures up to T_1 (red arrows) in zero field is displaced by a more dominant scattering mechanism upon increase of field. (*E*) At 4 T, an approximate $T^{1.6}$ power law (green line fit) is observed to extend down to zero temperature and is likely due to fluctuations associated with endpoint of the superconducting phase.

netic field and doping can drive the electronic system to quantum criticality in a similar but distinct manner. These two tuning parameters, one adding charge carriers and one breaking time reversal symmetry, likely alter the excitation spectrum in fundamentally different ways, as considered in the case of heavy-fermion systems with similar orthogonal tuning parameters (20). However, they also smoothly connect the ground state boundaries that define the phase diagram on the overdoped side.

In LCCO, resistivity data can be scaled as a function of $\Delta B/T$ as shown in Fig. 4, providing a second key signature of the reach of a quantum phase transition. First observed in heavy-fermion materials (21), this type of energy-temperature scaling not only indicates a quantum critical system below its upper critical dimension but also reflects the lack of an energy scale other than temperature itself (15). In such a case, the transport can be described generally as a function $f(\Delta B^{\gamma}/T)$ of both field and temperature, with asymptotic limits in both FL ($\Delta\rho \propto T^2$) and NFL ($\Delta\rho \propto T^n$) regions (*SI Text*). Through this approach, the anomalous T^n scattering and the magnetic field-tuned divergence of A_2 with exponent α are shown to be two aspects of the same critical behavior, with a self-consistency given by $\alpha = \gamma(2-n)$ that is derived in the *SI Text* (see Table 1 for summary of exponents). A scaling exponent γ is obtained for both $x = 0.15$ and 0.17, but with different values of 0.4 ± 0.1 for $x = 0.15$ (Fig. 4*C*) and 1.0 ± 0.02 for $x = 0.17$ (Fig. 4*D*). Given the same measured critical divergence exponent $\alpha = 0.38$ for both dopings, self-consistency requires that the power law exponent n must be different for these two dopings. Upon inspection of the phase diagram of Fig. 1, one can see this correspondence is indeed verified: At finite temperatures immediately above the quantum critical point at $B_c(x)$ for each doping, $\Delta\rho \propto T^n$ is best fit with $n = 1.0$ for $x = 0.15$, and $n = 1.6$ for $x = 0.17$ (Fig. 1), confirming self-consistency.

But what is the origin of these inherently different scattering rate behaviors, with $n = 1.0$ and $n = 1.6$? In LCCO, strong circumstantial evidence indicates that the temperature-linear scattering arises due to an antiferromagnetic quantum critical point that lies deep within the SC dome near $x_{FS} = 0.14$ (22, 23), where the Fermi surface reconstructs as in other electron-doped cuprates (24, 25). Fluctuations emanating from this critical point are likely to be responsible for the $n = 1.0$ power law (26) [strong disorder is evidenced by a small temperature-dependent change in $\rho(T)$ compared to ρ_0 in all cases], spawning an extended spin

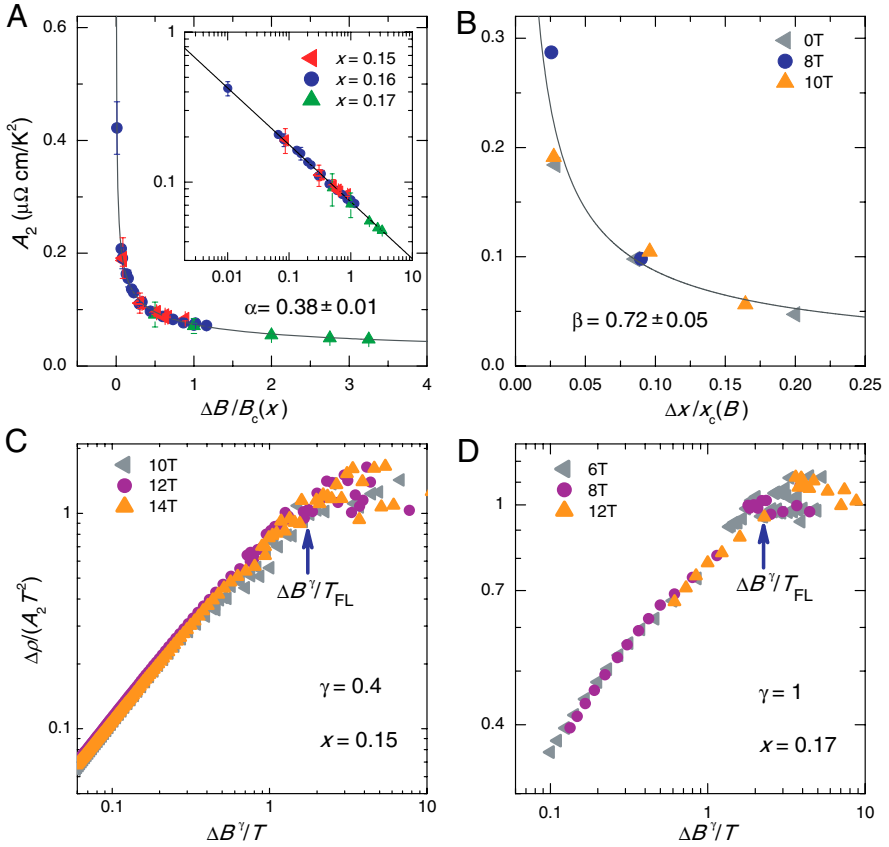

Fig. 4. Signatures of magnetic field and charge doping-tuned quantum criticality. (*A*) A strong increase of the quasiparticle–quasiparticle scattering coefficient A_2 (from fits of $\rho = \rho_0 + A_2T^2$) as a function of magnetic field provides evidence for a field-tuned quantum critical point, with a critical divergence observed to occur at the quantum critical field B_c as a function of the field tuning parameter $\Delta B = B - B_c$. Taken in the zero-temperature limit for three Ce concentrations spanning the overdoped region of superconducting LCCO, all of the data fit to one divergent function, $A_2 = A_0(\Delta B/B_c)^{-\alpha}$ with critical exponent $\alpha = 0.38 \pm 0.01$, indicating that the doping-dependent critical field $B_c(x)$ constitutes a quantum phase transition. The normalizing field-independent factor A_0 is equal to unity for $x = 0.15$, and scaled to unity for other samples to remove variations due to geometric factor uncertainties, and the inset presents the same data on a log–log plot with slope representative of the same exponent α. (*B*) A critical divergence in A_2 is also witnessed to occur as a function of Ce concentration tuning parameter $\Delta x = x - x_c$ upon approach to the critical doping x_c where the superconducting, Fermi liquid, and spin fluctuation phases terminate. Data for different magnetic field values are fitted by $A_2 = A_0(\Delta x/x_c)^{-\beta}$ with critical exponent $\beta = 0.72 \pm 0.05$, showing that A_2 diverges via two orthogonal tuning parameters that both cooperate to direct the evolution of $B_c(x)$ through the $T = 0$ field-doping plane (Fig. 1). The normalizing factor A_0 is equal to unity for 10 T data and scaled to unity for 0 T and 8 T value for the same reasons as above. (*C* and *D*) Scaling plots of $\rho(T)$ of LCCO for $x = 0.15$ and 0.17 in magnetic fields greater than B_c showing that resistivity $\Delta\rho$ data divided by A_2T^2 collapse onto the same curve with a suitable choice of scaling exponent γ. The blue arrows indicate $\Delta B^{\gamma}/T_{FL}$, which delineates the Fermi liquid side with zero slope and ordinate equal to unity from the non-Fermi liquid behavior with positive slope. The success of this scaling over two orders of magnitude in $\Delta B^{\gamma}/T$ indicates that the critical scaling of A_2 and the approximate T^n resistivity have the same origin, and that magnetic field and temperature are the dominant energy scales in the system.

Table 1. Definition and range of transport power law and critical exponents

Exponent	Determined by	Range of applicability	Value
n	power law fits to $\rho(T)$ data	temperature range depends on (x, B) (Fig. 1)	$1 < n < 2$
α	divergence of A_2 coefficients as B_c is approached from high B	all (x, B) exhibiting a Fermi liquid ground state	0.38 ± 0.01
β	divergence of A_2 coefficients as x_c is approached from high x	all (x, B) exhibiting a Fermi liquid ground state	0.72 ± 0.05
γ	collapse of $\rho(T)$ data for constant x at different values of B	all (x, B) exhibiting a Fermi liquid ground state, from 20 mK to upper limit of T^n behavior	$=\alpha(2\text{-}n)$, $\beta(2\text{-}n)=0.4 \pm 0.1 (x = 0.15)$ $=1.00 \pm 0.02 (x = 0.17)$

The dynamical range of the fitted parameter over which each exponent has been determined is shown explicitly in Fig. 1 for the transport power law exponent n, where temperature ranges of best fit are dependent on doping and field values (e.g., for $x = 0.15$, $n = 1$ for three decades of T in the range $0.020 < T < 20$ K). For the critical and scaling exponents, the dynamical ranges are shown explicitly in Fig. 4 and listed here for critical exponents α ($0.01 < \Delta B/B_c < 3$) and β ($0.025 < \Delta x/x_c < 0.20$), as well as the scaling exponent γ ($0.06 < \Delta B^{\gamma}/T < 10$ for $\gamma = 0.4$, and $0.1 < \Delta B^{\gamma}/T < 10$ for $\gamma = 1$).

fluctuation (SF) region defined by the $n = 1.0$ scattering behavior that dominates a substantial range of temperature, magnetic field, and doping. Of course, the inception of superconductivity likely consumes much of the entropy associated with such a state (27), filling in most of the SF phase space as shown in Fig. 2. However, as shown in Fig. 2*B*, a tantalizing glimpse of a possible non-Fermi liquid phase (NFL) may be present between the SC upper critical field B_{c2} and B_c, where an extended range of $T = 0$ NFL behavior endures much like in other anomalous systems (28–30).

Thus, at $x = 0.15$, the $n = 1.0$ scattering mechanism is dominant, extending to the zero-temperature limit once B_{c2} is surpassed, and the resultant $\Delta B/T$ scaling obeys the expected self-consistency in a wide range of fields and temperatures reaching up to the SF scale T_1. However, upon increasing doping from $x = 0.15$, the SF energy scale is dramatically reduced both in temperature and in field, with both scales terminating at the critical doping $x_c = 0.175$ where both T_1 and B_1 approach zero together with T_c and T_{FL}. Given the intimate correlation between T_1 and T_c in zero field (14), the discrepancy between their magnetic field dependence is all the more remarkable. It indicates that magnetic field does not destabilize superconductivity by destroying the mediating spin fluctuations, but rather through more mundane orbital effects. For instance, at $x = 0.15$, the upper temperature limit of the SF region, denoted as T_1, is much more robust against magnetic field than T_c itself, extrapolating to a zero-temperature field scale B_1 that far surpasses B_{c2} (Fig. 2*B*). But at higher doping, T_1 and T_c are both suppressed at an almost equal rate toward zero close to B_c, and the $n = 1.6$ power law characterizes the dominant scattering rate at temperatures directly above the quantum critical point. For instance, in the special case of $x = 0.17$ at 4 T (Fig. 2*C* and *SI Text*), this power law persists to at least 13 K, spanning at least three decades in temperature when it is the dominant scattering mechanism.

This correspondence underscores two major points. First, the magnetic field-induced divergence, critical scaling and the NFL scattering temperature dependence can be understood within a self-consistent framework. Second, the fact that this self-consistency adjusts according to which scattering is dominant is evidence for critical behavior arising from two origins—two sets of anomalous scattering, two forms of scaling and self-consistent critical exponents. Clearly, there are two distinct scattering behaviors that respond differently to doping and magnetic field, and the competition of these two scattering mechanisms is directly borne out in the temperature dependence of resistivity throughout the field-doping phase diagram. With the $n = 1.0$ power law likely arising from scattering with fluctuations associated with the antiferromagnetism of the parent compound, the $n = 1.6$ power law appears to be a distinct signature of a second type of quantum critical fluctuation. Interestingly, this power law is strikingly similar to that observed in the hole-doped cuprates $La_{2-x}Sr_xCuO_4$ (1) and $Tl_2Ba_2CuO_{6+x}$ (31) in the vicinity of x_c, suggesting the quantum critical endpoint of the SC phase may give rise to fluctuations that cause this particular anomalous scattering behavior. In fact, recent measurements of both $La_{2-x}Sr_xCuO_4$ (32) and $Tl_2Ba_2CuO_{6+x}$ (33) indeed show quantum critical behavior originating from the end of the SC dome, pointing to a universal nature of the quantum phase transition separating the superconducting and Fermi liquid ground states. The possibility of calculating a nonperturbative critical theory of such fluctuations for a disorder-driven SC quantum critical point (34) shows promise for confirming such a scenario.

Clearly, quantum criticality plays a significant role in shaping the phase diagram of the electron-doped cuprates, both in optimizing the superconductivity as well as limiting its extent. The ensuing picture is that two proximal quantum critical points compete in the cuprate phase diagram. The first, positioned near optimal doping, gives rise to spin fluctuations that stabilize unconventional superconductivity. The second, at $B_c(x)$, owes its very existence to the first because it is born of the suppression of superconductivity and the emergence of the normal FL state. The result is a complex but tractable interplay of competing quantum critical fluctuations that conspire to shape the phase diagram that has become the ubiquitous signature of high-temperature superconductivity.

Methods

Samples. The *c*-axis-oriented LCCO films were deposited on (100) $SrTiO_3$ substrates by pulsed laser deposition utilizing a KrF excimer laser. The annealing process for each Ce concentration was optimized such that samples showed the narrowest SC transition widths or metallic behavior down to the lowest measured temperature (20 mK), whereas nonoptimized samples usually showed an upturn at low temperature, as previously reported. The films were patterned into Hall bar bridges using photolithography and ion milling techniques. Several samples of each concentration were studied to ensure that the data are representative.

Measurements. Electrical transport measurements at temperatures greater than 2 K were carried out in a commercial cryostat equipped with a 14 T magnet, whereas lower temperature measurements down to 20 mK were performed in a dilution refrigerator equipped with a 15 T magnet. Data from the two platforms were measured with overlapping temperature ranges. Current was applied in the *ab* plane while the magnetic field was applied along the *c* axis for all the measurements.

ACKNOWLEDGMENTS. We thank A. Chubukov, V. Galitski, J. Schmalian, L. Taillefer, and C. M. Varma for their discussions. This research was supported by the National Science Foundation under DMR-0952716 (to J.P. and K.K.) and DMR-1104256 (to R.L.G.) and the Maryland Center for Nanophysics and Advanced Materials (K.J. and N.P.B.).

1. Cooper RA, et al. (2009) Anomalous criticality in the electrical resistivity of $La_{2-x}Sr_xCuO_4$. *Science* 323:603–607.

2. Taillefer L (2010) Scattering and pairing in cuprate superconductors. *Annu Rev Condens Matter Phys* 1:51–70.

3. Tanatar MA, Paglione J, Petrovic C, Taillefer L (2007) Anisotropic violation of the Wiedemann-Franz law at a quantum critical point. *Science* 316:1320–1322.
4. Maple MB, et al. (2010) Non-Fermi liquid regimes and superconductivity in the low temperature phase diagrams of strongly correlated *d*- and *f*-electron materials. *J Low Temp Phys* 161:4–54.
5. Sachdev S (2010) Where is the quantum critical point in the cuprate superconductors? *Phys Status Solidi B* 247:537–543.
6. Aji V, Shekhter A, Varma CM (2010) Theory of the coupling of quantum-critical fluctuations to fermions and *d*-wave superconductivity in cuprates. *Phys Rev B* 81:064515.
7. Broun DM (2008) What lies beneath the dome? *Nat Phys* 4:170–172.
8. Doiron-Leyraud N, et al. (2007) Quantum oscillations and the Fermi surface in an underdoped high- T_c superconductor. *Nature* 447:565–568.
9. Vignolle B, et al. (2008) Quantum oscillations in an overdoped high-T_c superconductor. *Nature* 455:952–955.
10. Matsui H, et al. (2007) Evolution of the pseudogap across the magnet-superconductor phase boundary of $Nd_{2-x}Ce_xCuO_4$. *Phys Rev B* 75:224514.
11. Kartsovnik MV, et al. (2011) Fermi surface of the electron-doped cuprate superconductor $Nd_{2-x}Ce_xCuO_4$ probed by high-field magnetotransport. *New J Phys* 13:015001.
12. Armitage NP, Fournier P, Greene RL (2010) Progress and perspectives on electron-doped cuprates. *Rev Mod Phys* 82:2421–2487.
13. Sawa A, et al. (2002) Electron-doped superconductor $La_{2-x}Ce_xCuO_4$: Preparation of thin films and modified doping range for superconductivity. *Phys Rev B* 66:014531.
14. Jin K, Butch NP, Kirshenbaum K, Paglione J, Greene RL (2011) Link between spin fluctuations and electron pairing in copper oxide superconductors. *Nature* 476:73–79.
15. Coleman P, Pépin C, Si Q, Ramazashvili R (2001) How do Fermi liquids get heavy and die? *J Phys Condens Matter* 13:R723–738.
16. Paglione J, et al. (2003) Field-induced quantum critical point in $CeCoIn_5$. *Phys Rev Lett* 91:246405.
17. Balicas L, et al. (2005) Magnetic field-tuned quantum critical point in $CeAuSb_2$. *Phys Rev B* 72:064422.
18. Gegenwart P, et al. (2002) Magnetic-field induced quantum critical point in $YbRh_2Si_2$. *Phys Rev Lett* 89:056402.
19. Nakatsuji S, et al. (2008) Superconductivity and quantum criticality in the heavy-fermion system β-$YbAlB_4$. *Nat Phys* 4:603–607.
20. Löhneysen Hv, Pfleiderer C, Pietrus T, Stockert O, Will B (2001) Pressure versus magnetic-field tuning of a magnetic quantum phase transition. *Phys Rev B* 63:134411.
21. Aronson MC, et al. (1995) Non-Fermi liquid scaling of the magnetic response of $UCu_{5-x}Pd_x$ ($x = 1, 1.5$). *Phys Rev Lett* 75:725–728.
22. Jin K, et al. (2009) Evidence for antiferromagnetic order in $La_{2-x}Ce_xCuO_4$ from angular magnetoresistance measurements. *Phys Rev B* 80:012501.
23. Jin K, et al. (2008) Normal-state transport in electron-doped $La_{2-x}Ce_xCuO_4$ thin films in magnetic fields up to 40 Tesla. *Phys Rev B* 77:172503.
24. Dagan Y, et al. (2004) Evidence for a quantum phase transition in $Pr_{2-x}Ce_xCuO_{4-\delta}$ from transport measurements. *Phys Rev Lett* 92:167001.
25. Lin J, Millis AJ (2005) Theory of low-temperature Hall effect in electron-doped cuprates. *Phys Rev B* 72:214506.
26. Rosch A (2000) Magnetotransport in nearly antiferromagnetic metals. *Phys Rev B* 62:4945–4962.
27. Wu J, Zhu L, Si Q (2011) Entropy accumulation near quantum critical points: Effects beyond hyperscaling. *J Phys Conf Ser* 273:012019.
28. Doiron-Leyraud N, et al. (2003) Fermi-liquid breakdown in the paramagnetic phase of a pure metal. *Nature* 425:595–599.
29. Butch NP, Maple MB (2009) Evolution of critical scaling behavior near a ferromagnetic quantum phase transition. *Phys Rev Lett* 103:076404.
30. Custers J, et al. (2010) Evidence for a non-Fermi-liquid phase in Ge-substituted $YbRh_2Si_2$. *Phys Rev Lett* 104:186402.
31. Shibauchi T, et al. (2008) Field-induced quantum critical route to a Fermi liquid in high-temperature superconductors. *Proc Natl Acad Sci USA* 105:7120–7123.
32. Lemberger TR, et al. (2011) Superconductor-to-metal quantum phase transition in overdoped $La_{2-x}Sr_xCuO_4$. *Phys Rev B* 83:140507(R).
33. Krusin-Elbaum L, et al. (2010) Interlayer magnetotransport in the overdoped cuprate $Tl_2Ba_2CuO_{6+x}$: Quantum critical point and its downslide in an applied magnetic field. *Phys Rev B* 82:144530.
34. Galitski V (2008) Nonperturbative microscopic theory of superconducting fluctuations near a quantum critical point. *Phys Rev Lett* 100:127001.

Supporting Information

Butch et al. 10.1073/pnas.1120273109

SI Text

Scaling of the Quadratic Coefficient A_2 of the Resistivity in the Fermi Liquid State. Fits to the electrical resistivity of the form $\rho = \rho_0 + A_2 T^2$ were performed on the high field side of B_c, i.e., in the field-induced Fermi liquid (FL) ground state. As a function of magnetic field, the data scale with identical critical exponent $\alpha = 0.38$. This analysis was performed on data from multiple samples at each concentration. In order to plot the data together in Fig. 4*A*, the absolute values of the coefficients for each sample were scaled by a constant value, which maintains the integrity of the scaling analysis. The necessity for rescaling is expected because of the sensitivity of the scattering to sample dependence beyond experimental control, which makes the success of the A_2 scaling all the more remarkable. A similar approach was used to put together Fig. 4*B*. Note that, experimentally, the step size is much coarser in the doping direction, and the uncertainty is larger due to the aforementioned sample dependence.

Resistivity Scaling Above the Fermi Liquid Boundary B_c. The scaling of $\rho(T)$ reflects the fact that the resistivity $\Delta\rho$ can be described generally as a function $A_2 T^2 f(\Delta B^\gamma/T)$, where $\Delta B = B - B_c$, that is applicable to scattering in both Fermi liquid ($\Delta\rho \propto T^2$) and non-Fermi liquid (NFL) ($\Delta\rho \propto T^n$) regions. In this framework, the T^n behavior in the NFL region stems from anomalous temperature dependence in A_2, which is by definition a constant in temperature in the FL state. The resultant picture is that T_{FL} separates the FL state at high magnetic field and low temperature from the NFL region at low magnetic field and high temperature, consistent with the magnetic field dependence of T_{FL} (Fig. 1*C*). This picture also suggests that upon crossing T_{FL} the dominant energy scale is transferred from temperature to magnetic field, which implicitly suggests that any dominant energy scale, such as Fermi energy, is absent.

The exponents α, γ, and n are related as $\alpha = \gamma(2 - n)$ by considering the following asymptotic limits: (*i*) Fermi liquid ($T \ll \Delta B$): $\Delta\rho = A_2(B)T^2$. In this limit, $\Delta\rho/A_2(B)T^2 = 1$ and thus $f(\Delta B^\gamma/T) \to 1$. (*ii*) Non-Fermi liquid ($T \gg \Delta B$):$\Delta\rho = A_n T^n = A_2(B)T^2 \times (\Delta B^\gamma/T)^{2-n}$. Our data show that when $n < 2$, $\Delta\rho < A_2(B)T^2$ and thus $f(\Delta B^\gamma/T) < 1$. Note that it is possible to define $A_2'(B, T) = A_2(B) \times (\Delta B^\gamma/T)^{2-n}$, or in other words, explicitly add a temperature dependence to A_2, which is a constant in temperature in the Fermi liquid state. However, from Fig. 4*A* we already know that $A_2 \propto \Delta B^\alpha$, and because A_2 and $A_2{}'$ must have the same magnetic field dependence, it follows that $\gamma(2 - n) = \alpha$.

For $x = 0.17$, scaling is satisfied using an exponent $\gamma = 1.0 \pm 0.02$, so $\alpha = 0.38$ forces $n \approx 1.6$. For $x = 0.15$, scaling is satisfied using an exponent $\gamma = 0.4 \pm 0.1$, so $\alpha = 0.38$ forces $n \approx 1.0$ (Fig. S4).

The plots in Fig. 4 show the difference between Fermi liquid and non-Fermi liquid behavior. In the Fermi liquid state, $\Delta\rho/A_2 T^2 = 1$ by definition, and the slope of the scaled curve is zero. In contrast, in the non-Fermi liquid regime the slope of the scaled curve is positive, reflecting the notion that A_2 is no longer a constant.

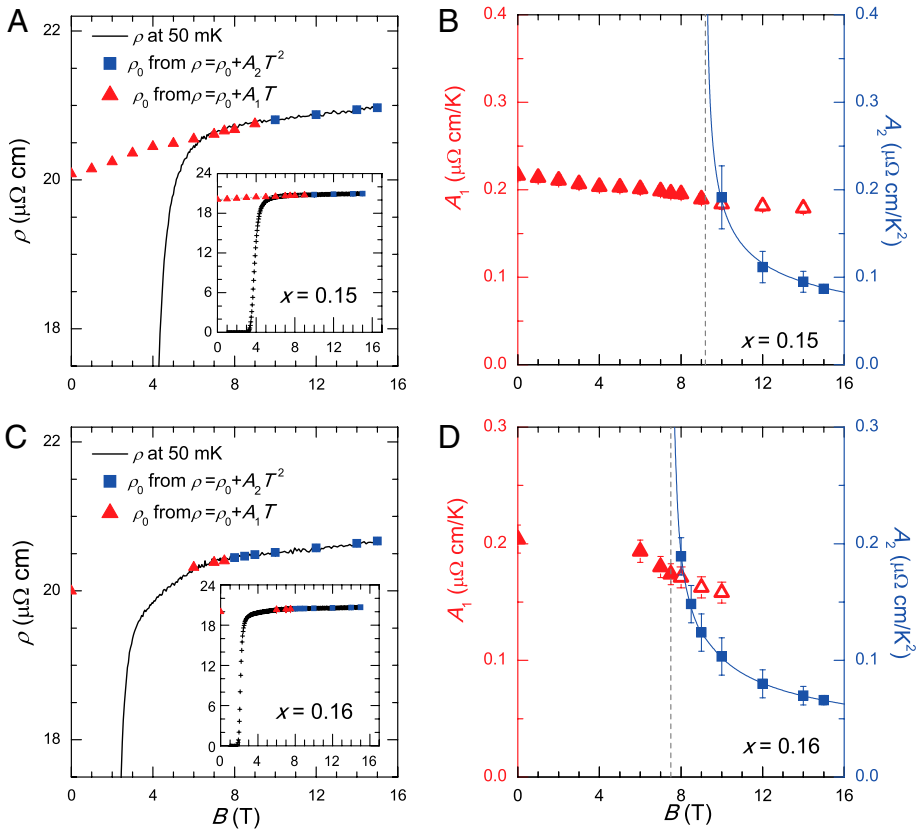

Fig. S1. Magnetic field dependence of resistivity ρ in the low temperature limit. *A* and *C* present vertical zooms of magnetoresistance data measured at a constant temperature of 50 mK for $x = 0.15$ and $x = 0.16$, respectively, and the residual ($T = 0$) resistivity ρ_0 obtained from extrapolated fits of $\rho(T)$ at different constant fields. Insets present the full vertical axis scales for each dataset. *B* and *D* present the field dependence of inelastic scattering coefficients A_1 (red) and A_2 (blue) for $x = 0.15$ and $x = 0.16$, respectively, demonstrating the persistence of finite-temperature $\Delta\rho \propto T$ scattering beyond the critical field (dashed line), which is the critical boundary of $\Delta\rho \propto T$ and $\Delta\rho \propto T^2$ regions at zero temperature. Note that although A_2 exhibits an upturn at the critical field, A_1 is completely insensitive to B_c.

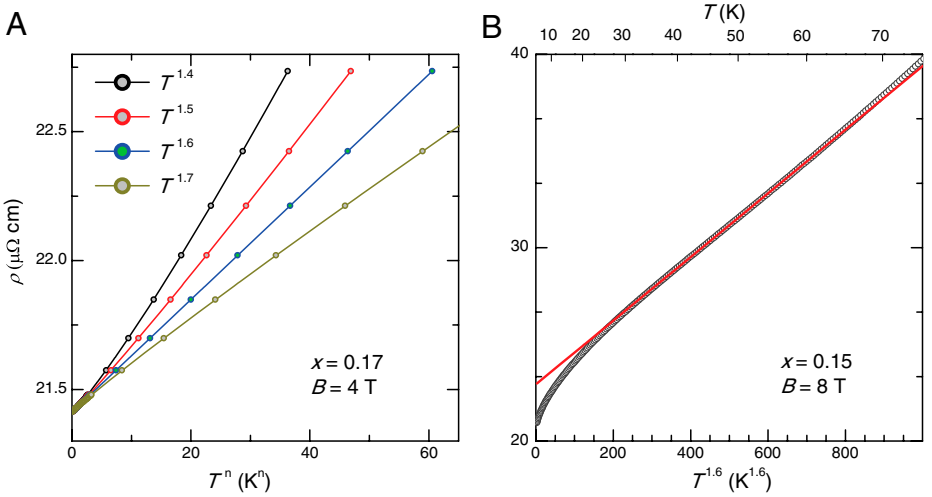

Fig. S2. Determination of $T^{1.6}$ resistivity. (*A*) Comparison of different power law temperature fits of the resistivity for $x = 0.17$ in a magnetic field of 4 T, where both $\Delta\rho \propto T$ and $\Delta\rho \propto T^2$ behaviors vanish. It is clear that a $T^{1.6}$ power yields the best fit, as shown by the blue data. (*B*) Demonstration of the range of the approximate $T^{1.6}$ power law fit for $x = 0.15$ in a field of 8 T, where $\Delta\rho \propto T$ behavior is dominant from zero temperature up to a cross-over temperature of approximately 20 K where the approximate $T^{1.6}$ power law becomes dominant and then extends up to approximately 60 K.

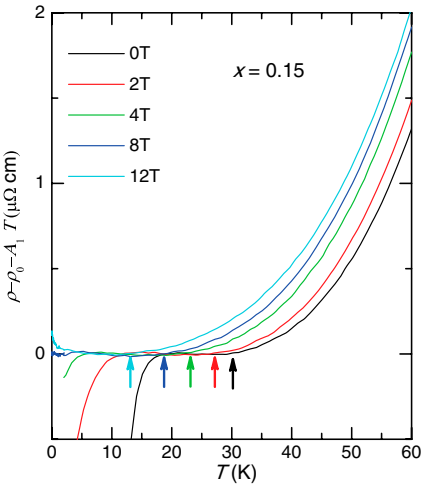

Fig. S3. Residuals of linear fits for $x = 0.15$. The definition of T_1 is denoted by arrows. Of particular note are the 8 T data (blue line) where temperature-linear resistivity extends from 20 mK up to approximately 20 K.

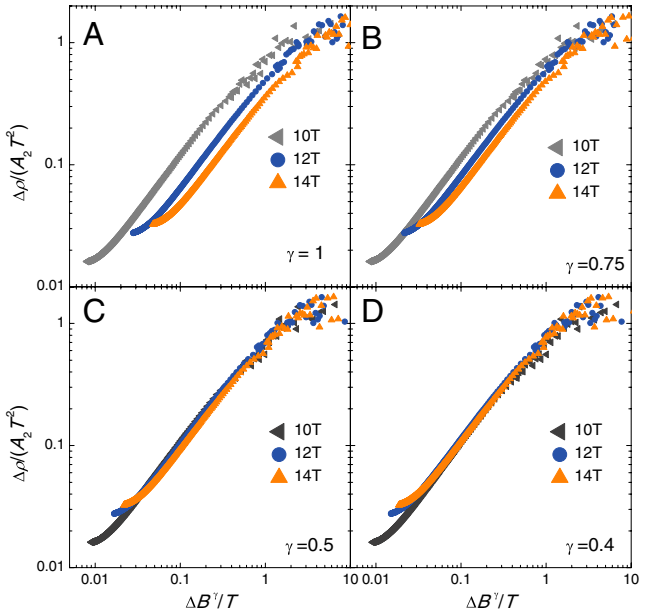

Fig. S4. Determination of resistivity scaling for $x = 0.15$. This series of plots demonstrates that γ should be considered as an independent fitting parameter and that the success of the scaling and its agreement with the critical scaling of A_2 as a function of B is a demonstration of self-consistency between the exponents. For instance, it is clear in *A* that the scaling exponent for $x = 0.15$ is not 1.0 (i.e., in contrast to the scaling observed for $x = 0.17$ with a choice of $\gamma = 1.0$, as shown in Fig. 4*D*).